ROLE OF DIFFERENT MODEL INGREDIENTS IN THE EXOTIC CLUSTER-DECAY OF ^{56}Ni*

N.K. DHIMAN

Govt. Sr. Sec. School, Summer Hill
(Shimla-171005, India; e-mail: narinder.dhiman@gmail.com)

PACS 25.70Jj, 23.70+j, 24.10-i, 23.60+e
©2012

We consider the cluster decay of ^{56}Ni* formed in heavy-ion collisions, by using different parameters proposed by different authors for the Fermi density distribution and the nuclear radius. Our study reveals that different technical parameters do not alter significantly the structure of fractional yields. The cluster decay half-lives of different clusters lie within ±10% for different Fermi density parameters and nuclear radii and, therefore, justify the current set of parameters used in the literature for the calculation of cluster decays.

1. Introduction

In earlier days, nuclei were considered to have a uniform density and sharp radius. With the passage of time, the density distribution was found to be more complicated. Several different forms (direct or indirect) exist in the literature, which can explain these complicated nuclear density distributions. The first method is the direct parametrization involving the choice of a suitable functional form, where parameters are varied to fit the experimental data. The two-parameter Fermi density distribution is an example of such a parametrization. The second method of indirect parametrization of a density distribution proceeds via nuclear models. A nuclear model like the shell model contains certain parameters, which are determined by other physical considerations, and it is then used to calculate the nuclear density distribution without further adjustments. The experimental data can be described accurately with the two-parameter Fermi density distribution at relatively low momenta. Among all the density distributions, the two-parameter Fermi density has been quite successful in the low, medium, and heavy mass regions. The systematic study of charge distributions have been carried out in [1–3]. We use this density distribution here.

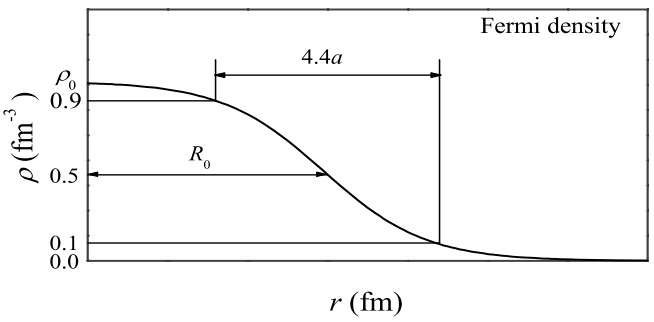

Fig. 1. Systematics diagram for the two-parameter Fermi density

Since the nuclear systems obey quantum laws, their surfaces are not well defined therefore. The nuclear density remains constant up to a certain distance but fall more rapidly close to the surface region, where the nucleons are free to move about. The nuclear densities provide an important information about the structure of nuclear matter at low energies and other important information regarding the equation of state at intermediate energies [4, 5].

Various methods have been developed for exploring the nuclear structure and the radius. The scattering of electrons or electrically charged high-energy particles is employed as a probe to explore the proton distribution of the nuclei (i.e., charge radii), whereas neutral nuclear probes such as neutrons will give the effect of nuclear forces over the nuclear surface (i.e., interaction radii). The charge radii are often used to extract the information about nuclear radii. The electron scattering experiments show that the charge distribution within a nucleus either follows the Fermi trapezoidal shape or modified Gaussian distribution. These studies have shown that the nuclear charge density does not decrease abruptly, but has a finite diffuseness.

A model that uses a density distribution such as the two-parameter Fermi density (as shown in Fig. 1) has to rely on the information about the nuclear radius (or half density radii R_0), central density ρ_0, and surface diffuseness (a). Interestingly, several different experimental, as well as theoretical, values of these parameters are available in the literature [6–11]. In addition, several different names such as central radii, equivalent sharp radii, root-mean-square radii, *etc.* have also been used in the literature to define different functional forms. The role of different radii was examined for exotic cluster decay

half-lives [12], and two different forms of radii were found to predict half-lives different by five orders of magnitude within the same theoretical model. Similarly, the use of different values of surface diffuseness also varies from author to author. The effect of these model ingredients on the fusion process at low incident energies have been studied in [13], where it was found that the effect of different radii is more than marginal, and, therefore, this parameter should be used with a more fundamental basis. Unfortunately, no systematic study is still available for the cluster decay process. In this paper, we plan to study the role of Fermi density parameters in the cluster decay of ^{56}Ni* formed in heavy-ion collisions. Such a study is still missing in the literature.

Heavy-ion reactions provide a very good tool to probe the nuclei theoretically. This includes the low-energy fusion process [14], intermediate energy phenomena [15], as well as the cluster-decay and/or formation of superheavy nuclei [16, 17]. In the last one decade, several theoretical models have been employed in the literature to estimate the half-life times of various exotic cluster decays of radioactive nuclei. These outcomes have also been compared with experimental data. Among all the models employed, the preformed cluster model (PCM) [18–20] is widely used to study the exotic cluster decay. In this model, the clusters/fragments are assumed to be preborn well before the penetration of the barrier. This is in contrast to the unified fission models (UFM) [21–23], where only the barrier penetration probabilities are taken into account. In either of these approach, one needs complete knowledge of nuclear radii and densities used in the potential.

Let us consider the cluster decay of ^{56}Ni formed as an excited compound system in heavy-ion reactions. Since ^{56}Ni has negative Q-value (or $Q_{\rm out}$), it is stable against both fission and cluster decay processes. However, if it is is produced in heavy-ion reactions depending on the incident energy and the angular momentum involved, the excited compound system could either undergo the fission, by decaying via cluster emissions, or reveal the resonance phenomenon. The nucleus ^{56}Ni has a negative $Q_{\rm out}$ with different values for various exit channels and, hence, would decay only if it were produced with sufficient compound nucleus excitation energy, $E^{*}_{\rm CN}$ $(= E_{\rm cm} + Q_{\rm in})$, to compensate for negative $Q_{\rm out}$, the deformation energy of the fragments E_d, their total kinetic energy (TKE), and the total excitation energy (TXE) in the exit channel as

$$E^{*}_{\rm CN} = \mid Q_{\rm out} \mid + E_d + {\rm TKE} + {\rm TXE} \qquad (1)$$

(see Fig. 2, where E_d is neglected because the fragments are considered to be spherical). Here, $Q_{\rm in}$ adds to the entrance channel kinetic energy $E_{\rm cm}$ of the incoming nuclei in their ground states.

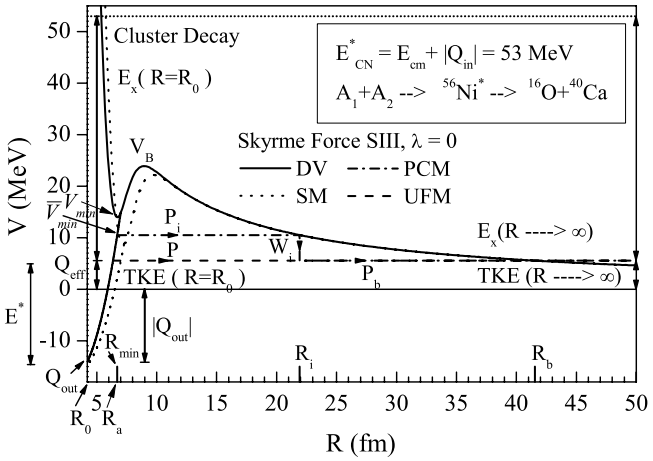

Fig. 2. Scattering potential $V(R)$ (MeV) for the cluster decay of ^{56}Ni* into ^{16}O + ^{40}Ca channel for different Fermi density parameters. The distribution of compound nucleus excitation energy $E^{*}_{\rm CN}$ at both the initial ($R = R_0$) and asymptotic ($R \to \infty$) stages and Q-values are shown. The decay path for both PCM and UFM models is also displayed

Section 2 gives some details of the Skyrme energy density model and the preformed cluster model and its simplification to the unified fission model. Our calculations for the decay half-life times of the ^{56}Ni compound system and a discussion of the results are presented in Section 3. Finally, the results are summarized in Section 4.

2. Model

2.1. Skyrme energy density model

In the Skyrme Energy Density Model (SEDM) [7], the nuclear potential is calculated as a difference of the energy expectation value E of the colliding nuclei at a finite distance R and at the complete isolation (i.e., at ∞) [7, 24],

$$V_N(R) = E(R) - E(\infty), \qquad (2)$$

where $E = \int H(\mathbf{r}) d\mathbf{r}$, with $H(\mathbf{r})$ as the Skyrme Hamiltonian density, which reads

$$H(\rho,\tau,\mathbf{J}) = \frac{\hbar^2}{2m}\tau + \frac{1}{2}t_0[(1+\frac{1}{2}x_0)\rho^2 - (x_0+\frac{1}{2})(\rho_n^2+\rho_p^2)] +$$

$$+\frac{1}{4}(t_1+t_2)\rho\tau + \frac{1}{8}(t_2-t_1)(\rho_n\tau_n+\rho_p\tau_p) +$$

$$+\frac{1}{16}(t_2-3t_1)\rho\nabla^2\rho + \frac{1}{4}t_3\rho_n\rho_p\rho +$$

$$+\frac{1}{32}(3t_1+t_2)(\rho_n\nabla^2\rho_n+\rho_p\nabla^2\rho_p)-$$

$$-\frac{1}{2}W_0(\rho\boldsymbol{\nabla}\cdot\mathbf{J}+\rho_n\boldsymbol{\nabla}\cdot\mathbf{J}_n+\rho_p\boldsymbol{\nabla}\cdot\mathbf{J}_p). \quad (3)$$

Here, $\mathbf{J}=\mathbf{J}_n+\mathbf{J}_p$ is the spin density, which was generalized in [7], for spin-unsaturated nuclei, and $\tau=\tau_n+\tau_p$ is the kinetic energy density calculated with the use of the Thomas–Fermi approximation [25,26], which reduces the dependence of the energy density $H(\rho,\tau,\mathbf{J})$ to be a function of the nucleon density ρ and the spin density $\mathbf{J}$ only. Here, the strength of the surface correction factor is taken to be zero (i.e. $\lambda=0$). The remaining term is the nucleon density $\rho=\rho_n+\rho_p$ and is taken to be the well-known two-parameter Fermi density. The Coulomb effects are neglected in the above energy density functional, but they will be added explicitly. In Eq. (3), six parameters t_0, t_1, t_2, t_3, x_0, and W_0 are fitted by different authors to obtain the best description of the various ground-state properties for a large number of nuclei. These different parametrizations have been labeled as S, SI, SII, SIII, *etc.* and are known as Skyrme forces for light and medium colliding nuclei. Other Skyrme forces are able to reproduce the data for heavy systems better. The Skyrme force used for the present study is SIII with the following parameters: $t_0=-1128.75$ MeV·fm^3, $t_1=395.00$ MeV·fm^5, $t_2=-95.00$ MeV·fm^5, $t_3=14000.00$ MeV·fm^6, $x_0=0.45$, and $W_0=120.00$ MeV·fm^5. It has been shown in previous studies that SIII force reproduces the fusion barrier much better than other sets of Skyrme forces for light and medium nuclei. However, other Skyrme forces such as SKa, SKm are found to be better for heavier masses. From Eq. (3), one observes that the Hamiltonian density $H(\rho,\tau,\mathbf{J})$ can be divided into two parts: (i) the spin-independent part $V_P(R)$, and (ii) spin-dependent $V_J(R)$ [7]:

$$V_N(R)=\int\{H(\rho)-[H_1(\rho_1)+H_2(\rho_2)]\}\,d\mathbf{r}+$$

$$+\int\{H(\rho,\mathbf{J})-[H_1(\rho_1,\mathbf{J}_1)+H_2(\rho_2,\mathbf{J}_2)]\}\,d\mathbf{r}=$$

$$=V_P(R)+V_J(R). \quad (4)$$

We apply the standard Fermi mass density distribution to the nucleon density:

$$\rho(R)=\frac{\rho_0}{1+\exp\left\{\frac{R-R_0}{a}\right\}},\quad -\infty\le R\le\infty. \quad (5)$$

Here, ρ_0, R_0, and *"a"* are respectively, the average central density, half-density radius, and surface diffuseness parameter. The R_0 gives a distance, where the density drops to a half of its maximum value, and the surface thickness s $(=4.4a)$ has been defined as a distance, over which the density drops from 90% to 10% of its maximum value that is the average central density ρ_0. The systematic two-parameter Fermi density distribution is shown in Fig. 1. Another quantity, which is equally important is the r.m.s. radius $\langle r^2\rangle_m$ defined as

$$\left\langle r^2\right\rangle_m=\int r^2\rho\left(\mathbf{r}\right)d\mathbf{r}=4\pi\int\limits_0^\infty\rho\left(\mathbf{r}\right)r^4d^3r. \quad (6)$$

One can find the half density radius by varying the surface diffuseness *"a"* and by keeping the r.m.s. radius $\langle r^2\rangle_m$ constant or from the normalization condition

$$R_0=\frac{1}{3}\left[5\left\langle r^2\right\rangle_m-7\pi^2a^2\right]. \quad (7)$$

The average central density ρ_0 is given by [27]

$$\rho_0=\frac{3A}{4\pi R_0^3}\left[1+\frac{\pi^2a^2}{R_0^2}\right]^{-1}. \quad (8)$$

Using Eq. (5), one can find the density of neutron and proton individually as:

$$\rho_n=\frac{N}{A}\rho,\quad \rho_p=\frac{Z}{A}\rho. \quad (9)$$

For the details of the model, the reader is referred to [7]. In order to see the effect of different Fermi density parameters on the cluster decay half-lives, we choose the following different Fermi density parameters proposed by various authors.

1. **H. de Vries *et al.* [11]:** Here, we use the interpolated experimental data [28] of L.R.B. Elton and H. de Vries for the half density radius R_0 and the surface thickness a. Using R_0 and a, the central density ρ_0 can be computed using Eq. (7). This set of parameters is labeled as DV.

2. **Ngô–Ngô [6]:** In the version of Ngô–Ngô, a simple analytical expression is used for nuclear densities instead of Hartree-Fock densities. These densities are taken to be of the Fermi type and written as

$$\rho_{n,p}(R)=\frac{\rho_{n,p}(0)}{1+\exp[(R-C_{n,p})/0.55]}, \quad (10)$$

$\rho_{n,p}(0)$ are then given by

$$\rho_n(0)=\frac{3}{4\pi}\frac{N}{A}\frac{1}{r_{0_n}^3},\quad \rho_p(0)=\frac{3}{4\pi}\frac{Z}{A}\frac{1}{r_{0_p}^3}, \quad (11)$$

where C represents the central radius of the distribution,

$$C = R\left[1 - \frac{1}{R^2}\right], \tag{12}$$

and

$$R = \frac{NR_n + ZR_p}{A}. \tag{13}$$

The sharp radii for a proton and a neutron are given by

$$R_p = r_{0_p}A^{1/3}, \quad R_n = r_{0_n}A^{1/3} \tag{14}$$

with

$$r_{0_p} = 1.128 \text{ fm}, \quad r_{0_n} = 1.1375 + 1.875 \times 10^{-4}A. \tag{15}$$

This set of parameters is labeled as Ngo.

3. **S.A. Moszkowski [8]:** The Fermi density parameters include, due to S.A. Moszkowski, the central density $\rho_0 = 0.16$ nucl./fm^3, the surface diffuseness parameter a equal to 0.50 fm, and radius $R_0 = 1.15A^{1/3}$. This set of parameters is labeled as SM.

4. **E. Wesolowski [9]:** The expressions for Fermi density parameters taken by E. Wesolowski read as follows. The central density

$$\rho_0 = \left[\frac{4}{3}\pi R_0^3\left\{1 + (\pi a/R_0)^2\right\}\right]^{-1}. \tag{16}$$

The surface diffuseness parameter $a = 0.39$ fm, and the half density radius

$$R_0 = R'\left[1 - \left(\frac{b}{R'}\right)^2 + \frac{1}{3}\left(\frac{b}{R'}\right)^6 + \ldots\right] \tag{17}$$

with

$$R' = \left[1.2 - \frac{0.96}{A^{1/3}}\left(\frac{N-Z}{A}\right)\right]A^{1/3}, \text{ and } b = \frac{\pi}{\sqrt{3}}\,a. \tag{18}$$

This set of parameters is labeled as EW.

5. **H. Schechter *et al.* [10]:** The value of Fermi density parameters taken by H. Schechter *et al.* can be summarized as: the central density $\rho_0 = 0.212/(1+2.66A^{-2/3})$, the surface diffuseness parameter a is equal to 0.54 fm, and the radius $R_0 = 1.04A^{1/3}$ in the single folding model for one of the nucleus. This set of parameters is labeled as HS.

In the spirit of the proximity force theorem, the spin independent potential $V_P(R)$ for the two spherical nuclei with radii C_1 and C_2 and with centers separated by a distance $R = s + C_1 + C_2$ is given by

$$V_P(R) = 2\pi\overline{R}\phi(s), \tag{19}$$

where

$$\phi(s) = \int \{H(\rho) - [H_1(\rho_1) + H_2(\rho_2)]\}\, dZ, \tag{20}$$

and

$$\overline{R} = \frac{C_1C_2}{C_1 + C_2}, \tag{21}$$

with Süssmann central radius C given in terms of the equivalent spherical radius R as

$$C = R - \frac{b}{R}. \tag{22}$$

Here, the surface diffuseness $b = 1$ fm, and the nuclear radius R is taken from the literature [6, 29–34].

In the original proximity potential [29], the equivalent sharp radius used is

$$R = 1.28A^{1/3} - 0.76 + 0.8A^{-1/3} \text{ fm}. \tag{23}$$

This radius is labeled as $\mathrm{R_{Prox77}}$.

In the present work, we also used the nuclear radius due to A. Winther labeled as R_{AW} [30]:

$$R = 1.20A^{1/3} - 0.09 \text{ fm}. \tag{24}$$

The newer version of the proximity potential uses a different formula for the nuclear radius [31]:

$$R = 1.240A^{1/3}\left[1 + 1.646A^{-1} - 0.191A_s\right] \text{ fm}. \tag{25}$$

This radius is labeled as R_{Prox00}.

Recently, a newer form of above Eq. (25) with slightly different constants is reported [32]:

$$R = 1.2332A^{1/3} + 2.8961A^{-2/3} - 0.18688A^{1/3}A_s \text{ fm}. \tag{26}$$

It is labeled as $\mathrm{R_{Royer}}$.

For the Ngô–Ngô [6] nuclear radius, we use Eqs. (13)–(15) and label it as R_{Ngo}.

The potential based on the classical analysis of experimental fusion excitation functions, used the nuclear radius (labeled as R_{Bass}) [33] as:

$$R = 1.16A^{1/3} - 1.39A^{-1/3}. \tag{27}$$

The empirical potential due to Christensen–Winther (CW) uses the same radius form (Eq. (27)) having different constants (labeled as R_{CW}) [34].

$$R = 1.233A^{1/3} - 0.978A^{-1/3}. \tag{28}$$

2.2. The preformed cluster model

For the cluster decay calculations, we use the Preformed Cluster Model [18–20]. It is based on the well-known quantum mechanical fragmentation theory [35–38] developed for the fission and heavy-ion reactions and used later on for predicting the exotic cluster decay [39–41]. In this theory, we have two dynamical collective coordinates of mass and charge asymmetry: $\eta = (A_1 - A_2)/(A_1 + A_2)$ and $\eta_Z = (Z_1 - Z_2)/(Z_1 + Z_2)$. The decay half-life $T_{1/2}$ and decay constant λ in the decoupled η- and R-motions satisfy the relation

$$\lambda = \frac{\ln 2}{T_{1/2}} = P_0 \nu_0 P, \tag{29}$$

where the preformation probability P_0 is referred to the η-motion, and the penetrability P to the R-motion. The quantity ν_0 is the assault frequency, with which the cluster hits the barrier. Thus, in contrast to the unified fission models [21–23], the two fragments in PCM are considered to be pre-born at a relative separation coordinate R before the penetration of the potential barrier with probability P_0. The preformation probability P_0 is given by

$$P_0(A_i) = \mid \psi(\eta, A_i) \mid^2 \sqrt{B_{\eta\eta}(\eta)} \left(\frac{4}{A_i}\right) \quad (i = 1 \text{ or } 2), \tag{30}$$

with $\psi^\nu(\eta), \nu = 0, 1, 2, 3, \ldots$, as solutions of the stationary Schrödinger equation in η at fixed R,

$$\left[-\frac{\hbar^2}{2\sqrt{B_{\eta\eta}}} \frac{\partial}{\partial\eta} \frac{1}{\sqrt{B_{\eta\eta}}} \frac{\partial}{\partial\eta} + V_R(\eta)\right] \psi^\nu(\eta) = E^\nu \psi^\nu(\eta), \tag{31}$$

solved at $R = R_a = R_{\min}$ at the minimum configuration, i.e., $R_a = R_{\min}$ (corresponding to $V_{\min}$) with the potential at this R_a-value as $V(R_a = R_{\min}) = \overline{V}_{\min}$ (displayed in Fig. 2).

The temperature effects are also included in this model through a Boltzmann-like function as

$$\mid \psi(\eta) \mid^2 = \sum_{\nu=0}^{\infty} \mid \psi^\nu(\eta) \mid^2 \exp\left(-\frac{E_\eta}{T}\right), \tag{32}$$

where the nuclear temperature T (in MeV) is equaled approximately to the excitation energy $E^*_{\rm CN}$:

$$E^*_{\rm CN} = \frac{1}{9} A T^2 - T, \quad \text{(in MeV)}. \tag{33}$$

The fragmentation potential (or collective potential energy) $V_R(\eta)$ in Eq. (31) is calculated within the Strutinsky renormalization procedure as

$$V_R(\eta) = -\sum_{i=1}^{2} \left[V_{\rm LDM}(A_i, Z_i) + \delta U_i \exp\left(-\frac{T^2}{T_0^2}\right)\right] +$$

$$+\frac{Z_1 \cdot Z_2 e^2}{R} + V_N(R), \tag{34}$$

where the liquid drop energies ($V_{\rm LDM} = B - \delta U$) with B as the theoretical binding energy of Möller *et al.* [42], and the shell correction δU is calculated in the asymmetric two-center shell model. The additional attraction due to the nuclear interaction potential $V_N(R)$ is calculated within SEDM potential using different Fermi density parameters and nuclear radii, as discussed earlier. The shell corrections are considered to vanish exponentially for $E^*_{\rm CN} \geq 60$ MeV, giving $T = 1.5$ MeV. The mass parameter $B_{\eta\eta}$ representing the kinetic energy part of the Hamiltonian in Eq. (31) is the smooth classical hydrodynamical mass by Kröger and Scheid [43].

The WKB action integral was solved for the penetrability P [41]. For each η-value, the potential $V(R)$ is calculated by using SEDM for $R \geq R_d$ with $R_d = R_{\min} + \Delta R$. For $R \leq R_d$, it is parametrized simply as a polynomial of degree two in R:

$$V(R) = \begin{cases} \mid Q_{\rm out} \mid + a_1(R - R_0) + a_2(R - R_0)^2 \\ \text{for} \quad R_0 \leq R \leq R_d, \\ V_N(R) + Z_1\, Z_2 e^2/R \\ \text{for} \quad R \geq R_d. \end{cases} \tag{35}$$

Here, R_0 is the parent nucleus radius, and ΔR is chosen for a smooth matching between the real potential and the parametrized potential (with second-order polynomial in R). A typical scattering potential calculated by using Eq. (35) is shown in Fig. 2, where the tunneling paths and the characteristic quantities are also marked. Here, we choose the first (inner) turning point R_a at the minimum configuration, i.e., $R_a = R_{\min}$ (corresponding to $V_{\min}$) with the potential $V(R_a = R_{\min}) = \overline{V}_{\min}$ at this R_a-value. The outer turning point R_b gives the $Q_{\rm eff}$-value of the reaction, $V(R_b) = Q_{\rm eff}$. This means that the penetrability P with the de-excitation probability $W_i = \exp(-bE_i)$ taken as 1 can be written as $P = P_i P_b$, where P_i and P_b are calculated, by using the WKB approximation, as

$$P_i = \exp\left[-\frac{2}{\hbar} \int_{R_a}^{R_i} \{2\mu[V(R) - V(R_i)]\}^{1/2} dR\right], \tag{36}$$

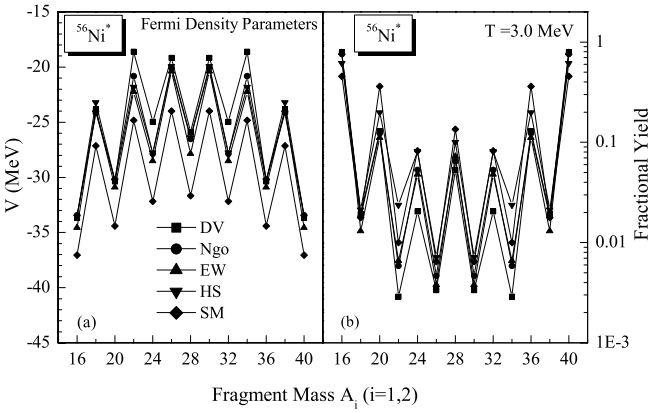

Fig. 3. (a) The fragmentation potential $V(\eta)$ and (b) the calculated fission mass distribution yield with different density parameters at $T = 3.0$ MeV

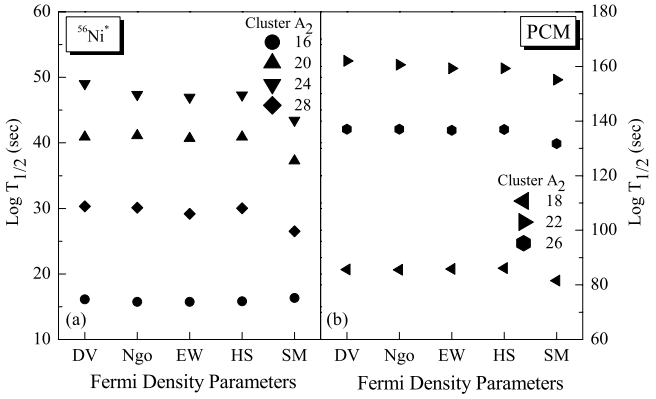

Fig. 4. Variation of $\log T_{1/2}$ (s) using different density parameters for PCM

and

$$P_b = \exp\left[-\frac{2}{\hbar}\int_{R_i}^{R_b}\{2\mu[V(R)-Q_{\rm eff}]\}^{1/2}dR\right]. \qquad (37)$$

Here, R_a and R_b are, respectively, the first and second turning points. This means that the tunneling begins at $R = R_a$ ($= R_{\rm min}$) and terminates at $R = R_b$ with $V(R_b) = Q_{\rm eff}$. The integrals in Eqs. (36) and (37) are calculated analytically by parameterizing the above-calculated potential $V(R)$.

The assault frequency ν_0 in Eq. (29) is given simply as

$$\nu_0 = \frac{v}{R_0} = \frac{(2E_2/\mu)^{1/2}}{R_0}, \qquad (38)$$

where $E_2 = \frac{A_1}{A}Q_{\rm eff}$ is the kinetic energy of the emitted cluster with $Q_{\rm eff}$ shared between the two fragments, and $\mu = m(\frac{A_1A_2}{A_1+A_2})$ is the reduced mass.

The PCM can be simplified to UFM, if the preformation probability $P_0 = 1$, and the penetration path is straight to $Q_{\rm eff}$-value.

3. Results and Discussions

In the following, we see the effect of different Fermi density parameters and nuclear radii on the cluster-decay process using the Skyrme energy density formalism within PCM and UFM.

First of all, to see the effect of different Fermi density parameters on the cluster decay half-lives, we choose the different Fermi density parameters proposed by various authors as discussed earlier.

Figure 2 shows the characteristic scattering potential for the cluster decay of ^{56}Ni* into the ^{16}O + ^{40}Ca channel as an illustrative example. In the exit channel for the compound nucleus to decay, the compound nucleus excitation energy $E^*_{\rm CN}$ is spent for compensating the negative $Q_{\rm out}$, total excitation energy TXE, and total kinetic energy TKE of two outgoing fragments as the effective Q-value (i.e., TKE= $Q_{\rm eff}$ in the cluster decay process). In addition, we plot the penetration paths for PCM and UFM using Skyrme force SIII (without surface correction factor, $\lambda = 0$) with DV Fermi density parameters. For PCM, we begin the penetration path at $R_a = R_{\rm min}$ with the potential $V(R_a = R_{\rm min}) = \overline{V}_{\rm min}$ at this R_a-value and ends at $R = R_b$, corresponding to $V(R = R_b) = Q_{\rm eff}$. Whereas, for UFM, we begin at R_a and end at R_b, both corresponding to $V(R_a) = V(R_b) = Q_{\rm eff}$. We have chosen only the case of the variable $Q_{\rm eff}$ (as taken in [44]) for different cluster decay products to satisfy the arbitrarily chosen relation $Q_{\rm eff} = 0.4(28- \mid Q_{\rm out} \mid)$ MeV, as it is more realistic [45]. The scattering potential with the SM Fermi density parameters is also plotted for comparison.

Figure 3,a and b shows the fragmentation potential $V(\eta)$ and the fractional yield at $R = R_{\rm min}$ with $V(R_{\rm min}) = \overline{V}_{\rm min}$. The fractional yields are calculated within PCM at $T = 3.0$ MeV using various Fermi density parameters for ^{56}Ni*. From the figure, we observe that the parameters play a minimal role in the fractional mass distribution yield. The fine structure is not varied at all for different sets of Fermi density parameters.

We have also calculated the half-life times (or decay constants) of ^{56}Ni* within PCM and UFM for clusters $\geq^{16}$O. For ^{16}O, the cluster decay constant varies by ten times. The variation is much more with SM parame-

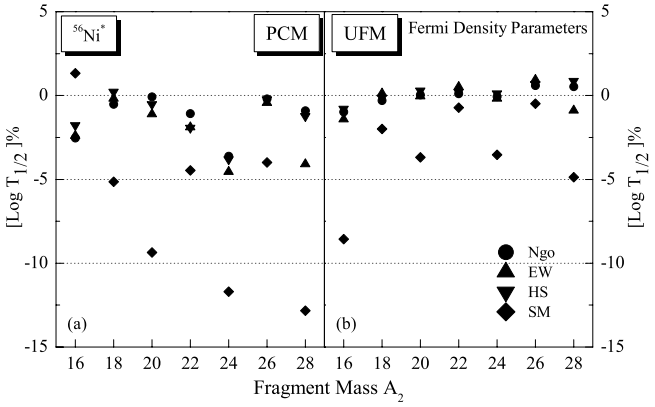

Fig. 5. Percentage variation of $\log T_{1/2}$ for different Fermi density parameters w.r.t. DV parameters

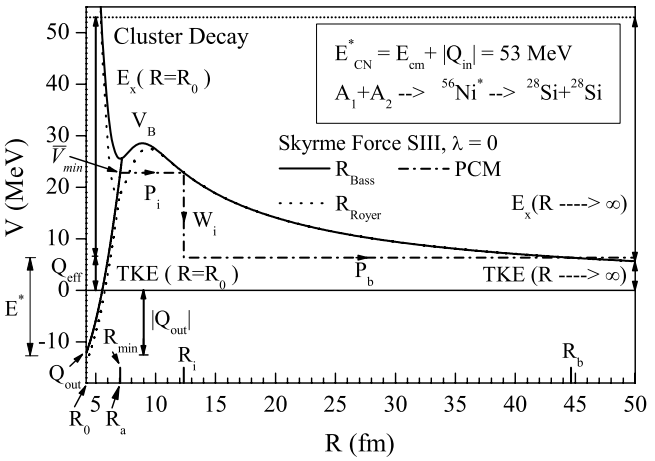

Fig. 6. Same as in Fig. 2, but for different radii. The decay path displayed only for PCM

ters. In the case of UFM, the variation is almost constant.

In Fig. 4, we display the cluster decay half-lives $\log T_{1/2}$ for various Fermi density parameters using PCM. There is a smooth variation in half-life times for all the density parameters except for the SM parameter. The trends in the variation of cluster half-life times (or decay constants) are similar in both PCM and UFM. But, in the case of the UFM decay, the constants are more by ten times. In SM, the decay constants are larger by 14 times.

In order to quantify the results, we have also calculated the percentage variation in $\log T_{1/2}$ as

$$\left[\log T_{1/2}\right]\% = \frac{(\log T_{1/2})^i - (\log T_{1/2})^{\rm DV}}{(\log T_{1/2})^{\rm DV}} \times 100, \qquad (39)$$

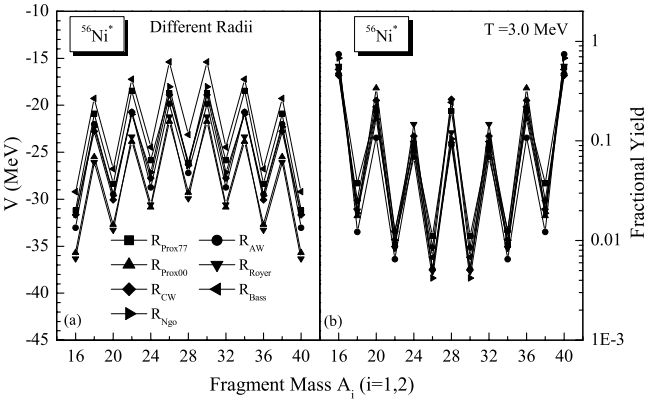

Fig. 7. Same as in Fig. 3, but for different radii

where i stands for the half-life times calculated using different Fermi density parameters. The variation in the cluster decay half-lives is studied with respect to DV parameters. In Fig. 5,*a* and *b*, we display the percentage variation in the half-life times within both the PCM and UFM models as a function of the cluster mass A_2, using Eq. (39). For PCM, this variation lies within $\pm 5\%$ excluding SM parameters, whereas it lies within $\pm 13\%$ with regard for SM parameters. In the case of UFM, the half-lives lie within $\pm 1.5\%$ for all density parameters, except for SM. For SM, the parameters variations lie within $\pm 9\%$.

Finally, it would be of interest to see how different forms of nuclear radii would affect, as was discussed earlier, the cluster decay half-lives.

In Fig. 6, we display the characteristic scattering potential for the cluster decay of ^{56}Ni* into the ^{28}Si + ^{28}Si channel for the $\mathrm{R_{Bass}}$ and $\mathrm{R_{Royer}}$ forms of nuclear radius. In the exit channel for the compound nucleus to decay, the compound nucleus excitation energy $E^*_{\rm CN}$ goes in compensating the negative $Q_{\rm out}$, the total excitation energy TXE and the total kinetic energy TKE of the two outgoing fragments as the effective Q-value. We plot the penetration path for PCM, by using the Skyrme force SIII (without the surface correction factor, $\lambda = 0$) with the nuclear radius $\mathrm{R_{Bass}}$. Here again, we begin the penetration path at $R_a = R_{\rm min}$ with the potential $V(R_a = R_{\rm min}) = \overline{V}_{\rm min}$ at this R_a-value and end at $R = R_b$, corresponding to $V(R = R_b) = Q_{\rm eff}$ for PCM. The $Q_{\rm eff}$ is same as discussed earlier.

Figure 7,*a* and *b* show the fragmentation potentials $V(\eta)$ and the fractional yields at $R = R_{\rm min}$ with $V(R_{\rm min}) = \overline{V}_{\rm min}$. The fractional yields are calculated within PCM at $T = 3.0$ MeV for ^{56}Ni*, by using various forms of nuclear radii. From the figure, we observe

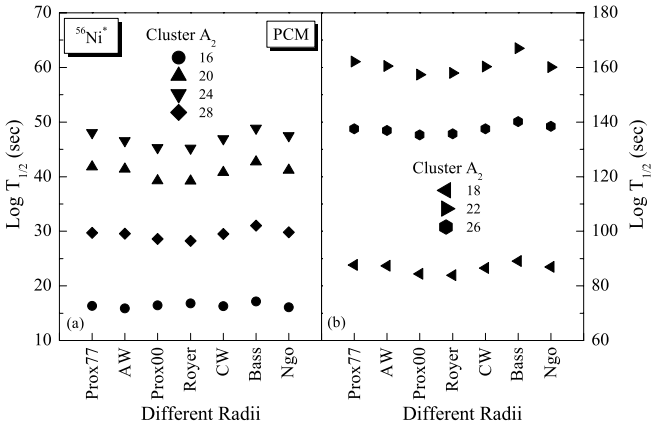

Fig. 8. Same as in Fig. 4, but for different radii

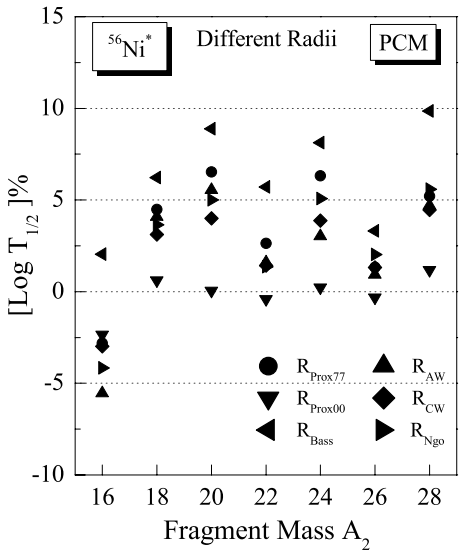

Fig. 9. Percentage variation of $\log T_{1/2}$ for different forms of radii with PCM only

that different radii give approximately a similar behavior. However, small changes in the fractional mass distribution yields are observed. The fine structure is not disturbed at all for different radius values.

We have also calculated the half-life times (or decay constants) of ^{56}Ni* within PCM for clusters $\geq^{16}$O. The cluster decay constant for the nuclear radius by R. Bass varies by 10^2, and the order of magnitude is same for other radii. In Fig. 8, we display the cluster decay half-lives $\log T_{1/2}$ for various nuclear radii taken by different authors, by using PCM. One can observe small variations in the half-life times.

In order to quantify the results, we have also calculated the percentage variation in $\log T_{1/2}$ as

$$\left[\log T_{1/2}\right]\% = \frac{(\log T_{1/2})^i - (\log T_{1/2})^{R_{\rm Royer}}}{(\log T_{1/2})^{R_{\rm Royer}}} \times 100, \quad (40)$$

where i stands for the half-life times calculated using different forms of nuclear radii. The variation in the cluster decay half-lives is studied with respect to the formula for radii $R_{\rm Royer}$ given by G. Royer. In Fig. 9, we display the percentage variation in the half-life times for PCM as a function of the cluster mass A_2, by using Eq. (40). This variation lies within $\pm 7\%$ excluding the Bass radius, where it lies within $\pm 10\%$.

4. Summary

We have reported the role of various model ingredients and radii in the cluster decay constant calculations. Our studies revealed that the effect of different densities and nuclear radii on the cluster decay half-life times is about 10%. Our study justifies the use of the current set of parameters for the radius, as the effect of different prescriptions is very small.

1. I. Angeli *et al.*, J. Phys. G: Nucl. Part. Phys. **6**, 303 (1980).
2. E. Wesolowski *et al.*, J. Phys. G: Nucl. Part. Phys. **10**, 321 (1984).
3. J. Friedrich and N. Vogler, Nucl. Phys. A **373**, 192 (1982).
4. S. Kumar *et al.*, Phys. Rev. C **58**, 3494 (1998); *ibid.* C **58**, 1618 (1998); J. Singh *et al.*, Phys. Rev. C **62**, 044617 (2000); E. Lehmann *et al.*, Phys. Rev. C **51**, 2113 (1995); R.K. Puri *et al.*, Nucl. Phys. A **575**, 733 (1994); D.T. Khoa *et al.*, Nucl. Phys. A **548**, 102 (1992); S.W. Huang *et al.*, Phys. Lett. B **298**, 41 (1993); G. Batko *et al.*, J. Phys. G: Nucl. Part. Phys. **20**, 461 (1994); S.W. Huang *et al.*, Prog. Part. Nucl. Phys. **30**, 105 (1993); E. Lehmann *et al.*, Prog. Part. Nucl. Phys. **30**, 219 (1993).
5. R.K. Puri *et al.*, Phys. Rev. C **54**, R28 (1996); *ibid.* J. Comput. Phys. **162**, 245 (2000); A. Sood *et al.*, Phys. Rev. C **70**, 034611 (2004); S. Kumar *et al.*, Phys. Rev. C **81**, 014601 (2010); *ibid.* C **78**, 064602 (2009); P.B. Gossiaux *et al.*, Nucl. Phys. A **619**, 379 (1997); C. Fuchs *et al.*, J. Phys. G: Nucl. Part. Phys. **22**, 131 (1996).
6. C. Ngô *et al.*, Nucl. Phys. A **252**, 237 (1975); H. Ngô and C. Ngô, Nucl. Phys. A **348**, 140 (1980).
7. R.K. Puri and N.K. Dhiman, Eur. Phys. J. A **23**, 429 (2005); R. Arora *et al.*, *ibid.* **8**, 103 (2000); R.K. Puri *et al.*, *ibid.* **3**, 277 (1998); R.K. Puri *et al.*, Phys. Rev. C **51**, 1568 (1995); *ibid.* **45**, 1837 (1992); *ibid.* J. Phys. G: Nucl.

Part. Phys. **18**, 903 (1992); R.K. Puri and R.K. Gupta, Int. J. Mod. Phys. E **1**, 269 (1992).

8. S.A. Moszkowski, Nucl. Phys. A **309**, 273 (1978).
9. E. Wesolowski, J. Phys. G: Nucl. Part. Phys. **11**, 909 (1985).
10. H. Schechter *et al.*, Nucl. Phys. A **315**, 470 (1979).
11. L.R.B. Elton, Nuclear Sizes, *Oxford Univ. Press, London* (1961); H. de Vries, C.W. de Jager, C.de Vries, At. Data Nucl. Data Tables **36**, 495 (1987).
12. R.K. Gupta *et al.*, J. Phys. G: Nucl. Part. Phys. **18**, 1533 (1992).
13. R. Arora, *Ph.D. Thesis* (Panjab University, Chandigarh, 2003).
14. J.M.B. Shorto *et al.*, Phys. Rev. C **81**, 044601 (2010); I. Dutt and R.K. Puri *ibid.* **81**, 047601 (2010); *ibid.* **81**, 044615 (2010); *ibid.* **81**, 064609 (2010); *ibid.* **81**, 064608 (2010).
15. C. Xu and B.A. Li, Phys. Rev. C **81**, 044603 (2010); S. Kumar *ibid.* **78**, 064602 (2008); *ibid.* **81**, 014611 (2010); *ibid.* **81**, 014601 (2010); Y.K. Vermani *et al.*, J. Phys. G: Nucl. Part. Phys. **36**, 105103 (2010); Y.K. Vermani *et al.*, *ibid.* **37**, 015105 (2010); Y.K. Vermani *et al.*, Europhys. lett. **85**, 62001 (2009); Y.K. Vermani *et al.*, Phys. Rev. C **79**, 064613 (2009); A. Sood *et al.*, *ibid.* **79**, 064618 (2009); S. Gautam *et al.*, J. Phys. G: Nucl. Part. Phys. **37**, 085102 (2010); S. Gautam *et al.*, Phys. Rev. C **83**, 014603 (2011); *ibid.* **83**, 034606 (2011); R. Chugh *et al.*, Phys. Rev. C **82**, 014603 (2010); S. Goyal *et al.*, Nucl. Phys. A **853**, 164 (2011); S. Goyal *et al.*, Phys. Rev. C **83**, 047601 (2011); V. Kaur *et al.*, Phys. Lett. B **697**, 512 (2011); V. Kaur *et al.*, Nucl. Phys. A **861**, 37 (2011).
16. S.K. Patra *et al.*, Phys. Rev. C **80**, 034612 (2009); S.K. Arun *et al.*, *ibid.* **80**, 034317 (2009); *ibid.* **79**, 064616 (2009); R. Kumar *et al.*, *ibid.* **79**, 034602 (2009).
17. K.P. Santhosh *et al.*, J. Phys. G: Nucl. Part. Phys. **36**, 115101 (2009); *ibid.* **36**, 015107 (2009); K.P. Santhosh *et al.*, Pramana J. Phys. **59**, 599 (2002).
18. R.K. Gupta, in *5th Intern. Conference on Nuclear Reaction Mechanisms, Varenna, Italy*, p. 416 (1988).
19. S.S. Malik and R.K. Gupta, Phys. Rev. C **39**, 1992 (1989); *ibid.* **50**, 2973 (1994); S.S. Malik *et al.*, Pramana J. Phys. **32**, 419 (1989); R.K. Gupta *et al.*, Phys. Rev. C **47**, 561 (1993).
20. S. Kumar and R.K. Gupta, Phys. Rev. C **55**, 218 (1997); *ibid.* **49**, 1922 (1994).
21. D.N. Poenaru, W. Greiner, and R. Gherghescu, Phys. Rev. C **47**, 2030 (1993); H.F. Zhang *et al.*, *ibid.* **80**, 037307 (2009).
22. B. Buck, A.C. Merchant, and S.M. Perez, Nucl. Phys. A **512**, 483 (1990); B. Buck and A.C. Merchant, J. Phys. G: Nucl. Part. Phys. **16**, L85 (1990).
23. A. Sandulescu *et al.*, Int. J. Mod. Phys. E **1**, 379 (1992); R.K. Gupta *et al.*, J. Phys. G: Nucl. Part. Phys. **19**, 2063 (1993); Phys. Rev. C **56**, 3242 (1997).
24. D. Vautherin and D.M. Brink, Phys. Rev. C **5**, 626 (1972).
25. P. Chattopadhyay and R.K. Gupta, Phys. Rev. C **30**, 1191 (1984), and references therein.
26. C.F. von Weizsäcker, Z. Phys. **96**, 431 (1935).
27. D.M. Brink and F. Stancu, Nucl. Phys. A **243**, 175 (1975); F. Stancu and D.M. Brink, *ibid*, A **270**, 236 (1976).
28. R.K. Puri, P. Chattopadhyay, and R.K. Gupta, Phys. Rev. C **43**, 315 (1991).
29. J. Blocki *et al.*, Ann. Phys. **105**, 427 (1977).
30. A. Winther, Nucl. Phys. A **594**, 203 (1995).
31. W.D. Myers and W.J. Światecki, Phys. Rev. C **62**, 044610 (2000).
32. G. Royer and R. Rousseau, Eur. Phys. J. A **42**, 541 (2009).
33. R. Bass, Phys. Lett. B **47**, 139 (1973).
34. P.R. Christensen and A. Winther, Phys. Lett. B **65**, 19 (1976).
35. R.K. Gupta *et al.*, J. Phys. G: Nucl. Part. Phys. **26**, L23 (2000).
36. R.K. Gupta, W. Scheid, and W. Greiner, Phys. Rev. Lett. **35**, 353 (1975).
37. D.R. Saroha, N. Malhotra, and R.K. Gupta, J. Phys. G: Nucl. Part. Phys. **11**, L27 (1985).
38. J. Maruhn and W. Greiner, Phys. Rev. Lett. **32**, 548 (1974).
39. A. Sandulescu, D.N. Poenaru, and W. Greiner, Sov. J. Part. Nucl. **11**, 528 (1980).
40. H.J. Rose and G.A. Jones, *Nature* **307**, 245 (1984).
41. R.K. Gupta and W. Greiner, Int. J. Mod. Phys. E **3**, 335 (1994).
42. P. Möller *et al.*, At. Data Nucl. Data Tables **59**, 185 (1995).
43. H. Kröger and W. Scheid, J. Phys. G: Nucl. Part. Phys. **6**, L85 (1980).
44. N.K. Dhiman and I. Dutt, Pramana J. Phys. **76**, 441 (2011).
45. M.K. Sharma, R.K. Gupta, and W. Scheid, J. Phys. G: Nucl. Part. Phys. **26**, L45 (2000).

Received 26.08.11

РОЛЬ РІЗНИХ СКЛАДОВИХ МОДЕЛІ
ДЛЯ ЕКЗОТИЧНОГО КЛАСТЕРНОГО РОЗПАДУ ^{56}Ni*

Н.К. Дхіман

Р е з ю м е

Розглянуто кластерний розпад ядра ^{56}Ni*, народженого в зіткненнях важких іонів. Використано різні параметри різних авторів для радіуса ядра і Фермі розподілу щільності. Показано, що різниця параметрів не змінює істотно структуру парціальних виходів. Періоди напіврозпаду для різних кластерів знаходяться в межах $\pm 10\%$ для різних параметрів для Фермі розподілу щільності і радіусів ядер і тому узгоджуються з набором параметрів, використовуваних в літературі для розрахунку кластерних розпадів.